ELSEVIER

Journal of Nuclear Materials 264 (1999) 99–112

journal of nuclear materials

Behaviour of fission gas in the rim region of high burn-up UO_2 fuel pellets with particular reference to results from an XRF investigation

M. Mogensen [a], J.H. Pearce [b], C.T. Walker [c,*]

[a] *Materials Department, Risø National Laboratory, P.O. Box 49, DK-4000 Roskilde, Denmark*
[b] *AEA Technology, Fuel Performance, Windscale, Seascale, Cumbria CA20 1PF, UK*
[c] *European Commission, Joint Research Centre, Institute for Transuranium Elements, P.O. Box 2340, D-76125 Karlsruhe, Germany*

Received 30 April 1998; accepted 8 July 1998

Abstract

XRF and EPMA results for retained xenon from Battelle's high burn-up effects program are re-evaluated. The data reviewed are from commercial low enriched BWR fuel with burn-ups of 44.8–54.9 GWd/tU and high enriched PWR fuel with burn-ups from 62.5 to 83.1 GWd/tU. It is found that the high burn-up structure penetrated much deeper than initially reported. The local burn-up threshold for the formation of the high burn-up structure in those fuels with grain sizes in the normal range lay between 60 and 75 GWd/tU. The high burn-up structure was not detected by EPMA in a fuel that had a grain size of 78 μm although the local burn-up at the pellet rim had exceeded 80 GWd/tU. It is concluded that fission gas had been released from the high burn-up structure in three PWR fuel sections with burn-ups of 70.4, 72.2 and 83.1 GWd/tU. In the rim region of the last two sections at the locations where XRF indicated gas release the local burn-up was higher than 75 GWd/tU.

1. Introduction

All existing X-ray fluorescence analysis (XRF) results for the concentration of retained xenon in nuclear fuel come from the Risø National Laboratory in Denmark, where the use of the technique was pioneered in the Second and Third Fission Gas Release Projects [1,2]. In contrast to electron probe microanalysis (EPMA), which measures the concentration of gas retained in the UO_2 lattice and in gas bubbles smaller than 0.1 μm, XRF gives the total amount of gas locally retained in a nuclear fuel, which includes the concentration trapped on grain boundaries and in large intergranular bubbles. This is because in XRF the depth of analysis is at least 18 μm [3]. Thus, by using both XRF and EPMA to measure the radial distribution of xenon in a nuclear fuel a detailed picture of the fission gas behaviour can be obtained which includes the local percentage released to the rod free volume, the local fraction of gas retained in the fuel grains and the local fraction of gas trapped on the grain boundaries [4].

One area in which XRF has shown great potential is in the elucidation of the total percentage of fission gas released from the high burn-up structure that forms in the surface region of UO_2 fuel when the local burn-up exceeds about 60 GWd/tU [5,6]. The structure, which shows a pronounced decrease in fuel grain size and a high density of small facetted pores [7], is characterised by the loss of fission gas from the fuel matrix [6,7] and is generally attributed to recrystallisation (see e.g. [8–10]). Under typical light water reactor (LWR) conditions the local burn-up threshold of 60 GWd/tU is reached at an average section burn-up of 40–45 GWd/tU. At this average burn-up, the high burn-up structure begins to form at the pellet rim where the local burn-up is highest due to the presence of fissile ^{239}Pu formed by neutron capture. With increase in pellet burn-up above 40–45 GWd/tU the area covered by the high burn-up structure

* Corresponding author. Tel.: +49-7247 951 477; fax: +49-7247 951 590.

0022-3115/99/$ – see front matter
PII: S0022-3115(98)00474-7

in the outer region of the fuel increases in size since the radial position at which the threshold burn-up is reached moves away from the fuel surface. The width of the transformed zone in the outer region in the fuel can be estimated from the distance over which pin hole porosity is observed in the optical microscope or from the depth to which xenon depletion in the fuel matrix is measured with the electron microprobe. A comparison of results from optical microscopy and EPMA has indicated that the latter method is more sensitive (it can reveal partially transformed regions not easily detected in the optical microscope) and hence gives zone widths for the high burn-up structure that are generally greater than those furnished by optical microscopy [5].

Unfortunately, only a few XRF measurements could be performed on fuel with an average burn-up higher than 45 GWd/tU before the equipment at the Danish National Research Centre was dismantled in 1990 when work on nuclear fuel was halted. Nevertheless, amongst the measurements are six analyses on fuel sections with average burn-ups in the range 55–83 GWd/tU made on behalf of the High Burn-up Effects Program (HBEP) [5,11]. This paper reviews and re-evaluates the XRF and EPMA results from these HBEP fuel sections. The data set is unique because it includes the only known XRF data for fuel with a burn-up higher than 50 GWd/tU. It also has a special significance because it is unlikely that new data will be added in the near future since no nuclear research facility in the world presently possesses the capability to carry out XRF on irradiated nuclear fuel. The main reason for re-examining the data was to discover whether fission gas escapes from the high burn-up structure to the rod free volume at high local burn-up. In addition to studying the fission gas behaviour, the opportunity was taken to further verify the local burn-up threshold for the high burn-up structure and to check its depth of penetration in the fuel sections. Cunningham et al. [12] report that the high burn-up structure did not extend further than $r/r_o = 0.95$. This is contrary to current understanding that the high burn-up structure can cover a large area when the pellet burn-up exceeds roughly 60 GWd/tU.

It is to be noted that the EPMA was performed by J.H. Pearce and C. Taylor at the UKAEA's Northern Laboratories at Windscale, and that J.F.W. Thompson and A.W. Bell also of the UKAEA's Northern Research Laboratories obtained the fuel ceramography results which have proved an important aid to the interpretation of the XRF and EPMA data in the HBEP reports.

2. The high burn-up effects program

The HBEP was managed by Battelle Pacific Northwest Laboratories in the USA and sponsored by 25 organisations which included fuel manufacturers, electrical utilities and goverment bodies from Europe, Japan and the USA. The Project began in 1978 and lasted 12 years, during which time 82 LWR fuel rods were irradiated to burn-ups between 22 and 69 GWd/tU and afterwards examined using a wide range of post-irradiation analysis techniques. The principal objective of the Program was to gather data on fission gas release at high burn-up. This information was required to validate the predictions made by fission gas release models in the fuel performance codes then currently in use. These models had been modified in the seventies to allow for a presumed increase in fission gas release at extended burn-up. Details about the organisation of the Program, the work performed and the results obtained can be found in Refs. [5,11].

3. The HBEP fuels examined by XRF and EPMA

3.1. Fuel pellet and rod design characteristics

XRF and EPMA were carried out on fuel samples from six rods. Four, BK365, 3-138, BSH-06 and BLH-64 were of PWR design, although their length was restricted to 1 m to permit their irradiation in the BR-3 reactor. The two remaining rods, H8/36-4 and H8/36-6, were full-length commercial BWR rods which had been irradiated in the Olkiluoto-1 reactor in Finland. The fuel pellet and rod design characteristics are given in Table 1. It is seen that all four PWR fuels were highly enriched. The rod BK365 contained annular pellets and the fuel in rod BLH-64 had an abnormally large grain size of 78 μm obtained by the addition of 0.46 wt% Nb_2O_5. BSH-06 and BLH-64 were two of sixteen rods manufactured by the project. These rods exhibited two major fabrication anomalies. First, the helium fill gas contained around 20% argon. Second, the fuel contained islands of highly enriched UO_2 ($\sim$90% ^{235}U) up to 100 μm in diameter. In comparison with the PWR rods, the two BWR rods contained low enriched fuel of small grain size. Moreover, the fuel pellets were of larger diameter and the pressure of the He fill gas was markedly lower.

3.2. Irradiation conditions

The irradiation conditions for the rods from which sections were cut for XRF and EPMA are summarised in Table 2. For the PWR rods the peak pellet burn-up ranged from 62.5 to 83.1 GWd/tU and the peak heat rating from 27 to 41 kWm^{-1}. For the BWR rods H8/36-6 and H8/36-4 the peak pellet burn-up was 51.4 and 54.9 GWd/tU and the peak heat rating was 30 and 24 kWm^{-1}. The power histories for all the rods are shown in Fig. 1. It is seen that for BK365, the rod with the highest burn-up; the average linear heat rating during the first 500 days of irradiation was markedly lower than

Table 1
Fuel pellet and rod design characteristics

	Fuel Identification Code			
	BK [a]	3- [b]	BSH/BLH [c]	H8/36 [d]
Rod type	PWR	PWR	PWR	BWR
Pellet design	Annular	Solid	Solid	Solid
Pellet dia. (mm)	8.19	8.04	8.08	9.94
Enrichment (%^{235}U)	7.1	8.3	7.9	1.4
Pellet density (%TD)	93.2	95.0	95.0	95.7
2D grain size (μm)	16	16	16 and 78 [e]	6.6 [f]
Diametrical gap (mm)	0.17	0.20	0.19	0.21
Cladding material	Zry-4	Zry-4	Zry-4	Zry-2
Fill gas [g]	He (2.88)	He (1.96)	He (2.24) [h]	He (0.37)

[a] Annular fuel fabricated by Fragema/ Commissariat à l'Energie Atomique (CEA), France.
[b] Fuel supplied by Belgonucleaire, Belgium.
[c] Fuel manufactured by the project.
[d] Commercial BWR fuel fabricated by ABB Atom, Sweden.
[e] BSH 16 μm, BLH 78 μm.
[f] As observed.
[g] Figure in parenthesis is the pressure in MPa at 0°C.
[h] Contaminated with about 20% argon.

Table 2
Irradiation conditions

Rod	Reactor	Burn-up, GWd/tU		Irradiation Time [a]	Max. rod power [b]
		Rod average	Peak pellet	(Days)	(kWm^{-1})
BK365	BR-3	69.4	83.1	1587 (4)	27
BSH-06	BR-3	59.8	72.2	1188 (3)	39
3-138	BR-3	55.8	69.2	1175 (3)	35
BLH-64	BR-3	52.2	62.5	1188 (3)	41
H8/36-4	Olkiluoto-1	46.6	54.9	1925 (6)	24
H8/36-6	Olkiluoto-1	44.6	51.4	1600 (5)	30

[a] Figure in parenthesis is the number of irradiation cycles.
[b] Peak pellet.

that for the other three PWR rods. It is also evident that the power histories of BSH-06 and BLH-64 were broadly similar with the average linear heat rating during the first irradiation cycle varying between 29 and 34 kW m^{-1} before decreasing to between 10 and 15 kW m^{-1} in the third and final cycle.

3.3. Fuel temperature

Knowledge of the fuel temperature is an aid to the interpretation of the Xe distribution profiles measured by XRF and EPMA. From centre-line temperature measurements made under transient conditions in the Third Risø Fission Gas Release Project [2] it appears that the threshold temperature for thermal fission gas release from UO_2 fuel is close to 1200°C [13]. In the HBEP, the peak centre-line temperatures in the fuel rods were estimated from the power histories shown in Fig. 1 and the axial power profiles in the rods during each irradiation cycle using revision 2 of the GAPCON-THERMAL-2 code [14]. The computer calculations revealed that the fuel temperature was above 1200°C for the longest period in the BWR rods and that the temperature histories of these rods were such as to have had probably the greatest impact on fission gas release. For example, for rod H8/36-4 it was calculated that the peak centre-line temperature fluctuated around 1200°C in the first and second irradiation cycles, jumped to almost 1600°C in the third, varied between 1000°C and 1300°C in the fourth and fifth cycles and was around 700°C in the sixth and final cycle. In contrast, the temperature of the annular fuel pellets in rod BK365 was found to have exceeded 1000°C only in the first 100 days of the irradiation before significant burn-up had been accumulated and when the fission gas inventory was low. During the remainder of the irradiation the fuel temperature was calculated to have been generally below 800°C. For BSH-06 the peak centre-line temperature was apparently well above 1200°C in the first cycle and the first half of the second cycle, approaching 1600°C for about 100

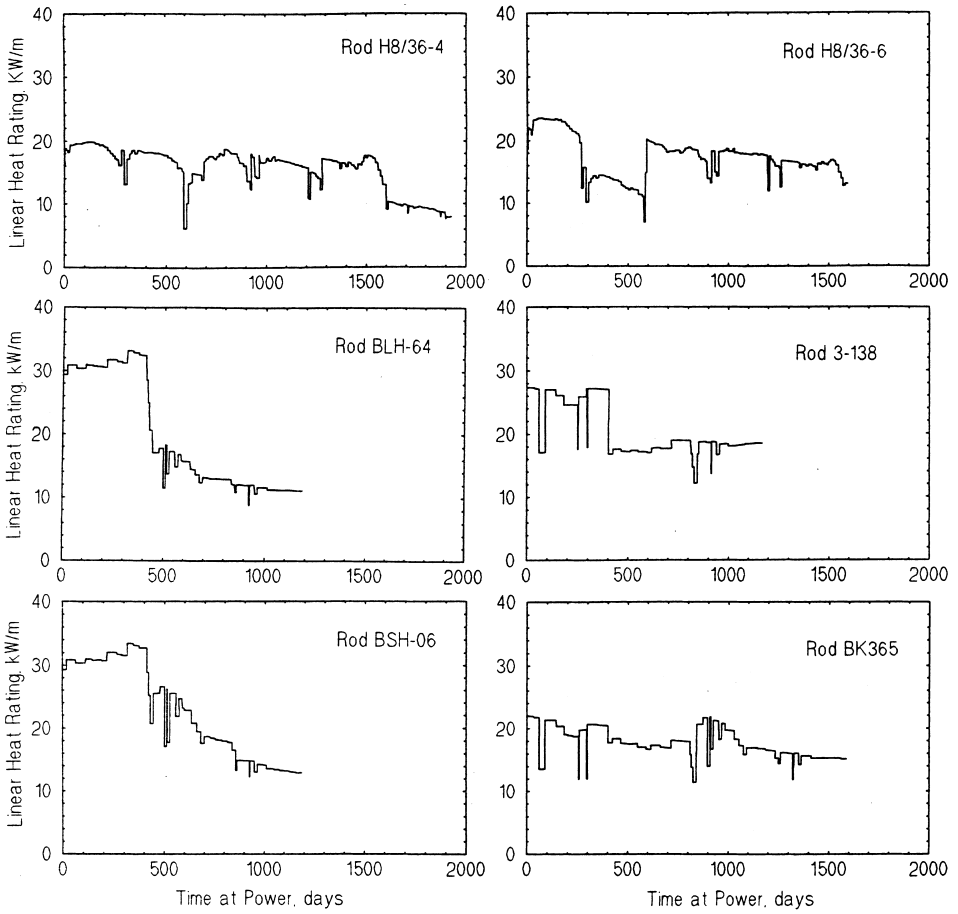

Fig. 1. Power histories for the six rods from which sections were cut for XRF and EPMA.

days at one point. It then decreased gradually to about 700°C at the end of the irradiation. For rod BLH-64, the calculated peak centre-line temperature was also well above 1200°C during the first cycle. It was, however, already below 800°C at the beginning of the second cycle.

4. Methods

The fuel sections analysed by XRF and EPMA are listed in Table 3. It is seen that XRF was carried out on sections close to those used for EPMA. In most cases, the fuel section used for XRF was about 1 cm (i.e., about one pellet) distance from the one on which EPMA was carried out. Thus, the same burn-up was reported for the EPMA and XRF sections from the same rod, although the axial gamma-scans for some rods indicate that a slight difference in burn-up could exist. XRF measurements of the radial xenon distribution were

Table 3
Fuel sections examined by XRF and EPMA

Fuel section [a]	Burn-up (GWd/tU)	EPMA	XRF
BK365-45	83.1		•
BK365-46	83.1	•	
BSH-06-48	72.2		•
BSH-06-49	72.2	•	
3-138-49	70.4		•
3-138-50	70.4	•	
BK365-85	67.1		•
BK365-86	67.1	•	
BLH-64-40	62.5		•
BLH-64-43	62.5	•	
H8/36-4-222	54.9		•
H8/36-4-220.5	54.9	•	
H8/36-6-215	50.9		•
H8/36-6-216	50.9	•	
H8/36-4-48	44.8		•
H8/36-4-48.2	44.8	•	

[a] The last number is the axial distance of the section from the bottom of the fuel stack in cm.

made on only two BR-3 fuel sections (BSH-06-48 and BLH-64-40). In the case of the other three BR-3 sections, XRF was confined to the rim region between $r/r_o = 0.95$ and the pellet surface.

4.1. X-ray fluorescence analysis

X-ray fluorescence analysis was carried out using a 50 kV primary beam produced by a RIGACU® rotating anode, high intensity X-ray generator. The beam was 4 mm long and 100 mm wide and impinged on the sample surface at an angle of 45°. The intensity of the Xe Kα line in the X-ray spectrum was measured using a solid state germanium detector. A collimator confined the area analysed to 0.35×4 mm^2 with the short dimension aligned in the direction of traverse across the fuel section. To reduce the radiation background, the collimated fluorescent X-rays were deflected 3.5° by a graphite crystal inserted between the collimator and the detector [3].

The XRF specimens were longitudinal fuel wafers 100–200 μm thick. The radial distribution of xenon was constructed from intensity measurements made on diametral specimens at intervals of 0.25 or 0.50 mm. The acquisition time was approximately 22 min. The local xenon concentration profile in the rim region was determined on specimens taken in the vicinity of the fuel surface. These wafers cut the fuel surface at a low angle, significantly increasing the depth resolution. For example, 1.3 mm on the rim specimen BK365-45 approximated to a radial distance in the fuel pellet of just 200 μm. As a result of the increase in depth resolution 15 xenon determinations could be made in the radial interval between the pellet surface and $r/r_o = 0.95$. The intensity of the U Lα line was measured at the same time as the Xe Kα X-ray intensity and used to reveal the presence of wide cracks and to pinpoint the position of the fuel pellet surface. The depth of analysis was taken to be 18 μm. At this depth 37% (e^{-1}) of the X-rays generated were emitted from the specimen. A gas standard consisting of xenon at a pressure of 0.9 bar was used to convert the measured X-ray intensity to an absolute concentration. X-ray absorption in the irradiated fuel was assumed to be equal to that in pure UO_2.

The uncertainty on a xenon concentration of 0.5 wt% is estimated to be 10% relative (1σ). This uncertainty level has been established in part by comparing the measured concentrations in the outer region of numerous fuel sections (burn-up <45 GWd/tU) with the generated concentration calculated from the burn-up and in part by repeating the analysis of a reference fuel specimen. One major source of uncertainty is the poor reproducibility of the count rate from the gaseous standard which is thought to be related to changes in the atmospheric pressure and the ambient temperature. For the rim specimens, the calculated radial locations corresponding to the positions where XRF was carried out are precise to better than ±0.001 on the relative radius scale (equal to approximately ±5 μm) and the width of the analysed area (0.35 mm) corresponds to a radial distance of about 15 μm.

4.2. Electron probe microanalysis

EPMA was carried out on a JEOL 733 microprobe with computer control provided by a LINK energy dispersive system (AN10000 with SPECTRA software). An electron acceleration potential of 15 kV and a beam current of 150 nA were used. Xenon was analysed using the approach employed at the Institute for Transuranium Elements [15]. This involved using antimony as a standard for xenon and applying a correction factor. The correction factor was derived by interpolating the intensity for pure solid xenon from the intensities for the adjacent elements in the periodic table. In addition to xenon, a number of other fission products were analysed including neodymium which was taken as a burn-up indicator. Also, the local concentrations of plutonium and uranium were analysed. The concentrations of these elements are required for the EPMA matrix correction. The backscattered or secondary current image was used to obtain information about the fuel microstructure at the locations selected for analysis and to position the electron beam. During analysis the beam was scanned over a small area measuring 10×50 μm. (Area analysis was favoured because it led to less scatter in the data.) For xenon and neodymium a PET diffracting crystal was employed and the counting time on the specimen peak and background was 100 s. The EPMA matrix correction was made with a ZAF routine in the LINK software.

The confidence interval on the measured xenon concentrations at the 95% level (2σ) was typically 0.025 wt%. For neodymium a similar level of uncertainty is expected. This interval is based solely on the statistics of X-ray counting. It does not take into account the distribution in the concentration obtained at each radial position as a result of making multiple determinations, or calibration errors.

5. Reliability of the XRF and EPMA data

5.1. Data handling

To check the reliability of the data the average integral concentrations of neodymium and xenon calculated from the measured radial concentration profiles were used. The neodymium concentration measured by EPMA was used to verify the reported burn-up. The consistency of the xenon data obtained by EPMA and XRF was checked by comparing the fission yield values

calculated from the radial profile for the amount of xenon created. Since fission gas release had occurred in the central region of all but one of the fuels analysed, this profile was reconstructed from the radial neodymium profile. The latter was adjusted to the level of the EPMA xenon profile in the outer region of the fuel and the created amount of xenon was then obtained by volume integration. When this approach was not possible, owing to the scatter in the data (section 3-138-50) or because gas release had occurred in the outer region of the fuel (sections BK365-46 and BK365-86), the neodymium profile was positioned at the level of the xenon data point with the highest concentration.

5.2. General observations

A systemic error in the EPMA measurements has resulted in a general underestimation of the concentration of neodymium in the fuel cross-sections. It is seen from Table 4 that for the low enriched fuel irradiated in the Olkiluoto-1 reactor 0.07–0.08 wt% neodymium is equivalent to a burn-up of 10 GWd/tU, whereas for the high enriched fuel irradiated in BR-3 0.08–0.09 wt% neodymium is equivalent to 10 GWd/tU. Both these concentration levels are below the value of 0.10–0.12 wt% expected for high burn-up UO_2 fuel [6].

The created concentration of xenon derived from the EPMA and XRF radial profiles, and the equivalent fission yield calculated from these concentrations are shown in Tables 5 and 6. It is seen that the calculated fission yield is in all cases well below the usual value of around 0.26 [16]. For six of the thirteen fuel sections analysed a xenon yield close to 0.20 or 0.21 was calculated and for three further sections a yield between 0.23 and 0.24 was calculated. Particularly low values were obtained for the fuel sections H8/36-6-216 (0.167), H8/36-4-220 (0.176), BSH-06-49 (0.189) and BSH-06-48 (0.175). Since a similar range of yield values is found for the two types of fuel it is concluded that the uncertainties on the EPMA and XRF data are mainly responsible for the general underestimation of the fission yield for xenon and for the spread in the calculated yield values.

6. XRF and EPMA radial concentration profiles

Only the fuel sections with an average burn-up of 54.9 GWd/tU and above are considered in this section. The XRF and EPMA profiles for the radial distribution of xenon in the fuel sections from rods H8/36-4, BLH-64 and BSH-06 are compared in Figs. 2, 3 and 6. In these

Table 4
Concentration of neodymium measured by EPMA and the concentration equivalent to a burn-up of 10 GWd/tU

Fuel section [a]	Burn-up (GWd/tU)	Measured Nd conc. [a] (wt%)	wt% per 10 GWd/tU
BK365-46	83.1	0.725	0.087
BSH-06-49	72.2	0.598	0.083
3-138-50	70.4	0.645	0.091
BK365-86	67.1	0.612	0.091
BLH-64-43	62.5	0.564	0.090
H8/36-4-220.5	54.9	0.428	0.078
H8/36-6-216	50.9	0.348	0.069
H8/36-4-48.2	44.8	0.357	0.080

[a] Cross-section integral average concentration.

Table 5
Created concentration of xenon derived from the EPMA radial profiles and the equivalent fission yield

Fuel section	Burn-up		Created Xe conc. [a]	Xe fission yield
	(GWd/tU)	% FIMA [b]	(wt%)	
BK365-46	83.1	8.7	0.867	0.201
BSH-06-49	72.2	7.6	0.713	0.189
3-138-50	70.4	7.4	0.788	0.215
BK365-86	67.1	7.1	0.745	0.212
BLH-64-43	62.5	6.6	0.680	0.208
H8/36-4-220.5	54.9	5.8	0.509	0.176
H8/36-6-216	50.9	5.4	0.447	0.167
H8/36-4-48.2	44.8	4.7	0.548	0.233

[a] Cross-section integral average concentration neglecting fission gas release.
[b] Assuming that 1% FIMA = 9.5 GWd/tU (i.e., 203 MeV per fission).

Table 6
Created concentration of xenon derived from the XRF radial profiles and the equivalent fission yield

Fuel Section	Burn-up		Created Xe Conc. [a]	Xe fission yield
	(GWd/tU)	% FIMA [b]	(wt%)	
BSH-06-48	72.2	7.6	0.661	0.175
BLH-64-40	62.5	6.6	0.765	0.234
H8/36-4-222	54.9	5.8	0.594	0.206
H8/36-6-215	50.9	5.4	0.539	0.201
H8/36-4-48	44.8	4.7	0.543	0.233

[a] Cross-section integral average concentration neglecting fission gas release.
[b] Assuming that 1% FIMA = 9.5 GWd/tU (i.e., 203 MeV per fission).

figures the profiles have been put at the same level for the purposes of comparison. This involved a small displacement of either the XRF or EPMA profile of less than 0.09 wt%. For the sections from rods 3-138 and BK365 where XRF was restricted to the rim region, the measured EPMA and XRF concentrations are used in Figs. 4, 5 and 7.

6.1. Fuel sections H8/36-4-220.5 and -222 (54.9 GWd/tU)

As seen in Fig. 2 a near perfect match exists between the XRF and EPMA profiles. Only in the rim region between $r/r_o = 0.97$ and the pellet surface do the profiles deviate significantly. The inflexion in the EPMA profile at $r/r_o = 0.97$ marks the limit of penetration of the high burn-up structure. The fact that the XRF profile follows closely the increase in burn-up in the vicinity of the fuel rim is taken as evidence that most, if not all, of the xenon missing from the new grains was contained in the fine pores of the high burn-up structure.

6.2. Fuel sections BLH-64-40 and -43 (63.5 GWd/tU)

It is seen from Fig. 3 that in the central region of the fuel and in the outer part of the fuel between $r/r_o = 0.75$ and 0.97 there is a good match between the XRF and EPMA profiles. In the central region of the fuel thermal gas release had occurred and in the zone between $r/r_o = 0.5$ and 0.75 XRF measured far higher concentrations of retained xenon than EPMA showing that fission gas was trapped in the grain boundary porosity in this region. At the pellet rim the EPMA profile does not fall, but increases with the local burn-up indicating that the high burn-up structure has not formed although the local burn-up at the pellet rim had exceeded 80 GWd/tU.

6.3. Fuel sections BK365-85 and -86 (67.1 GWd/tU)

The EPMA and XRF results for these two sections of annular fuel are shown in Fig. 4. In the outer region of the fuel between $r/r_o = 0.66$ and the pellet surface the

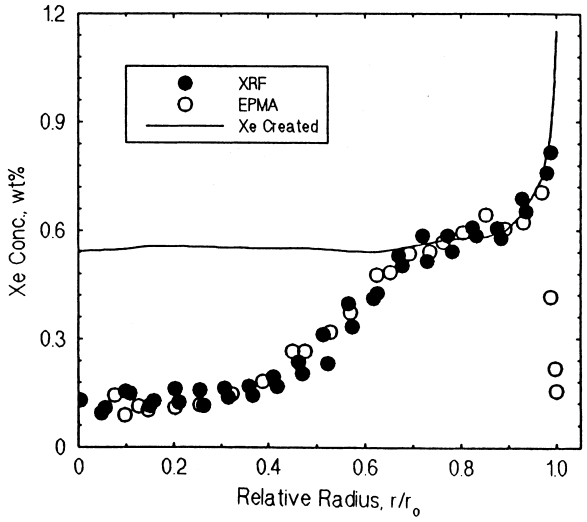

Fig. 2. Radial distribution of xenon in the fuel section H8/36-4-222 as revealed by XRF and in fuel section H8/36-4-220.5 as revealed by EPMA. The EPMA profile has been adjusted to the level of the XRF profile for the purposes of comparison. Burn-up 54.9 GWd/tU.

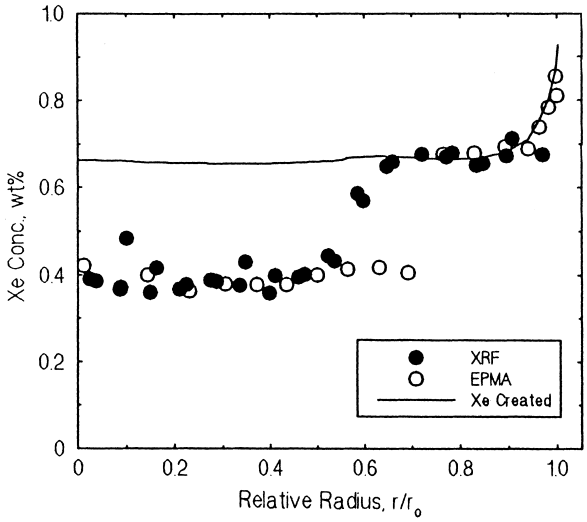

Fig. 3. Radial distribution of xenon in fuel section BLH-64-40 as revealed by XRF and in fuel section BLH-64-43 as revealed by EPMA. The XRF profile has been adjusted to the level of the EPMA profile for the purposes of comparison. Formation of the high burn-up structure has been impeded by the large grain size (78 μm). Burn-up 62.5 GWd/tU.

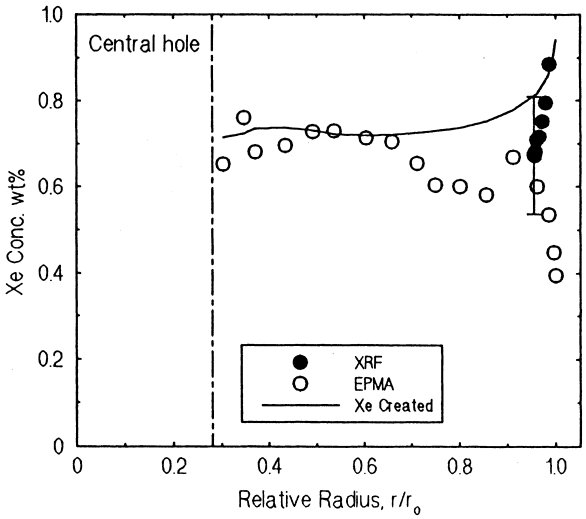

Fig. 4. Radial distribution of xenon in fuel section BK365-85 as revealed by XRF and in fuel section BK365-86 as revealed by EPMA. The error bar on the XRF concentrations marks the confidence limits at the 99% level (3σ). Burn-up 67.1 GWd/tU.

xenon concentrations measured by EPMA lie consistently below the line representing the amount of xenon created. The inflexion in the EPMA profile at $r/r_o = 0.66$ marks the limit of penetration of the high burn-up structure. The burn-up at this radial position calculated from the local neodymium concentration was 64.8 GWd/tU. The XRF profile is seen to fall sharply with distance from the pellet rim. The first XRF data point at $r/r_o = 0.99$ sits on the line for the amount of xenon created, and the last measurement at $r/r_o = 0.954$ is located on the EPMA profile.

6.4. Fuel sections 3-138-49 and -50 (70.4 GWd/tU)

As seen from Fig. 5, in the central region of the pellet the EPMA data points lie well below the profile for the created xenon concentration indicating that appreciable thermal fission gas release had occurred. The decrease in the xenon concentration at $r/r_o = 0.76$ marks the limit of penetration of the high burn-up structure. The neodymium concentration at this point indicates a local burn-up of 69.2 GWd/tU. The XRF measurements made in the region between $r/r_o = 0.95$ and the pellet

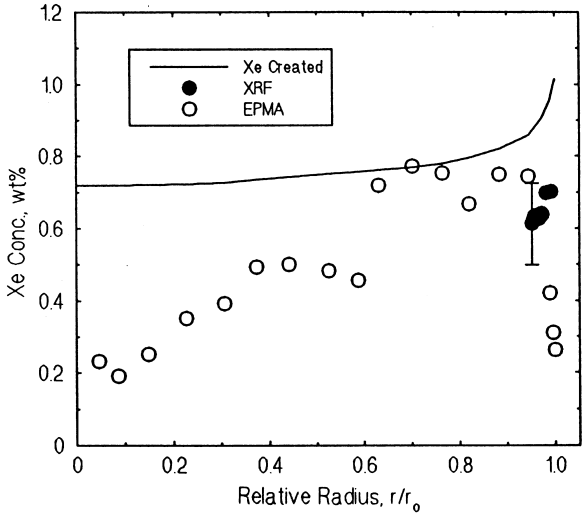

Fig. 5. Radial distribution of xenon in fuel section 3-138-49 as revealed by XRF and in fuel section 3-138-50 as revealed by EPMA. The error bar on the XRF concentrations marks the confidence limits at the 99% level (3σ). Burn-up 70.4 GWd/tU.

surface also lie well below the line for the amount of xenon created suggesting that fission gas has been released from the high burn-up structure to the rod free volume.

6.5. Fuel sections BSH-06-48 and -49 (72.2 GWd/tU)

As seen from Fig. 6, the XRF and EPMA profiles show that thermal gas release had occurred in the central region of the fuel and that an appreciable amount of gas was retained on the grain boundaries in the region between $r/r_o = 0.55$ and 0.75. In the outer region of the fuel where the high burn-up structure had formed all the gas released from the UO_2 grains had left the fuel. In this region the coincidence between the EPMA and XRF profiles is quite remarkable and at the pellet surface both exhibit a similar down turn. At $r/r_o = 0.85$, the deviation of the XRF and EPMA profiles from the line representing the created amount of xenon marks the limit of penetration of the high burn-up structure. At this radial position the burn-up determined from the local concentration of neodymium was 69.4 GWd/tU.

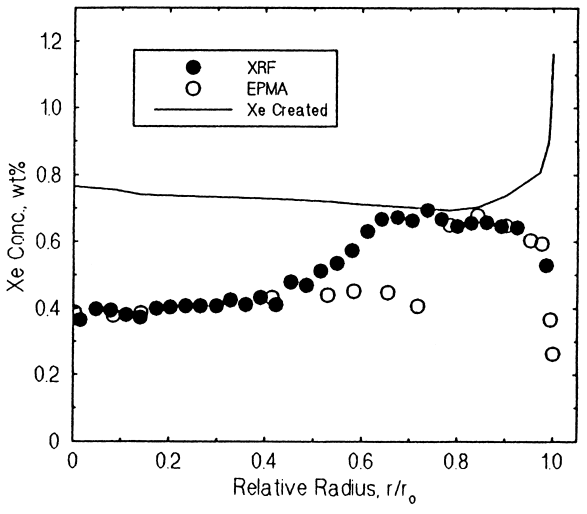

Fig. 6. Radial distribution of xenon in fuel section BSH-06-48 as revealed by XRF and in fuel section BSH06-49 as revealed by EPMA. The XRF profile has been adjusted to the level of the EPMA profile for the purposes of comparison. Burn-up 72.2 GWd/tU.

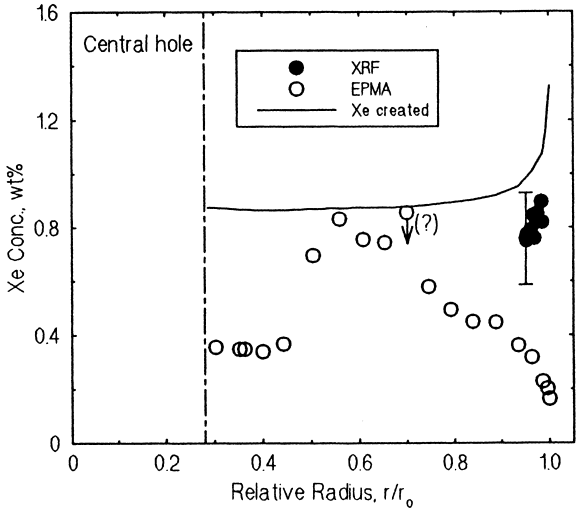

Fig. 7. Radial distribution of xenon in fuel section BK365-45 as revealed by XRF and in fuel section BK365-46 as revealed by EPMA. The high burn-up structure extends over the whole pellet cross-section. The error bar on the XRF concentrations marks the confidence limits at the 99% level (3σ). Burn-up 83.1 GWd/tU.

6.6. Fuel sections BK365-45 and -46 (83.1 GWd/tU)

It can be seen from Fig. 7 that in section BK365-46 the xenon concentrations measured by EPMA approach the created level only over a short distance at intermediate radial positions. On either side of this narrow band extending from $r/r_o = 0.55$ and 0.65 a substantial percentage of the xenon inventory had been released from the fuel grains in the central and outer regions of the fuel. Again, it is seen that the XRF data in the rim region of the pellet lie well above the measured EPMA concentrations but below the line representing the concentration of xenon created.

7. Discussion

7.1. Depth of penetration of the high burn-up structure

In Table 7 values obtained in this work for the depth of penetration of the high burn-up structure are compared with those reported by Cunningham et al. [12]. It is seen that in the four sections with average burn-ups higher than 65 GWd/tU the high burn-up structure penetrated much deeper than initially reported. In section BK365-46 with a burn-up of 83.1 GWd/tU it appears to have covered the whole pellet cross-section, although at intermediate radial positions the microstructure transformation was incomplete. This view stems from the ceramography results which revealed that the pin hole porosity, which is a feature of the high burn-up structure, was also present in the central region of the pellet (see Fig. 8). It is also supported by the knowledge that after the first 100 days, the fuel temperature did not rise above 800°C and thus was far below the threshold temperature of about 1200°C for thermal fission gas release [13]. Moreover, it is to be noted that Une et al. [17] likewise report finding that the high burn-up structure extended over almost the entire cross-section of the annular pellet in section BK365-46. Their finding results from SEM and ceramography investigations which were part of a detailed examination of the section carried out outside the frame of the HBEP by the Nippon Fuel Development Company, Japan. In these investigations new grains formed by recrystallisation were directly observed in the vicinity of the central hole.

It is also evident from Table 7 that in section BLH-64-43 the high burn-up structure had not developed to the extent it had in the other sections, even though the pellet burn-up was 62.5 GWd/tU. The large grain size of the fuel in this section (78 μm compared with 7 and 16 μm in the other sections) appears to have impeded the formation of the high burn-up structure. The effect might be a consequence of a decrease in the number of

Table 7
Depth of penetration of the high burn-up structure as found in this work and as reported by Cunningham et al.

Fuel section	Burn-up	Depth of penetration, μm	
	(GWd/tU)	Cunningham et al. [12]	This work
BK365-46	83.1	140	2900 [a]
BSH-06-49	72.2	198	660
3-138-50	70.4	221	960
BK365-86	67.1	160	1410
BLH-64-43	62.5	73	100 [b]
H8/36-4-220	54.9	159	150
H8/36-4-48.2	44.8	159	150

[a] The high burn-up structure extended from the pellet rim to the surface of the central hole.
[b] Ceramography shows patches of pin hole porosity at the pellet rim which could be associated with the formation of the high burn-up structure.

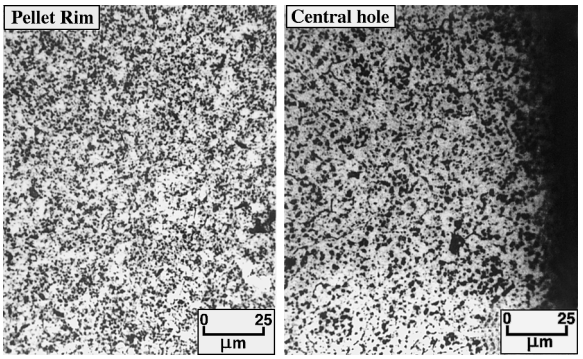

Fig. 8. Photomicrographs showing the microstructure of the fuel in the vicinity of the pellet rim and central hole in section BK365-46. The pin hole porosity which is a feature of the high burn-up structure is present at both locations. Etchant: 10% H_2SO_4 in concentrated H_2O_2 solution.

nucleation sites for recrystallisation caused by the decrease in grain boundary area. Another reason could be that large grains accumulate fewer irradiation induced defects than smaller grains as reported by Nogita and Une [18]. This implies that higher burn-ups are required to reach the level of lattice strain needed for recrystallisation. A further explanation may be associated with the presence of Nb_2O_5 which was added to the fuel to promote the formation of large grains. It is has been reported [19] that the presence of 0.5 wt% Nb_2O_5 in UO_2 increases the diffusion coefficient of xenon in large grained fuel by about a factor of 50. If this is so, Nb_2O_5 may also increase the mobility of point defects in the outer region of the fuel with the result that the recovery of irradiation damage is enhanced and recrystallisation avoided.

7.2. The threshold burn-up for the high burn-up structure

The threshold burn-up for the formation of the high burn-up structure has been determined following the approach used in a previous publication of one of the authors (CTW) [6]. This involves plotting the xenon concentrations measured by EPMA in the region between $r/r_o = 0.7$ and the pellet surface against the local burn-up. The threshold burn-up corresponds to the peak in the resulting concentration curve. The outcome of such a plot for the BR-3 and BWR fuels considered in this work is shown in Fig. 9. It is seen that the threshold burn-up for the formation of the high burn-up structure lies in the range 60–75 GWd/tU. This burn-up range is similar to that found for commercial pressurised water reactor (PWR) fuel [6]. The identification of a threshold burn-up and the fact that it is similar to that in PWR fuel is taken as confirmation that in the sections with an average burn-up greater than 65 GWd/tU the high burn-up structure extended over much of the outer region of the fuel (see Table 7).

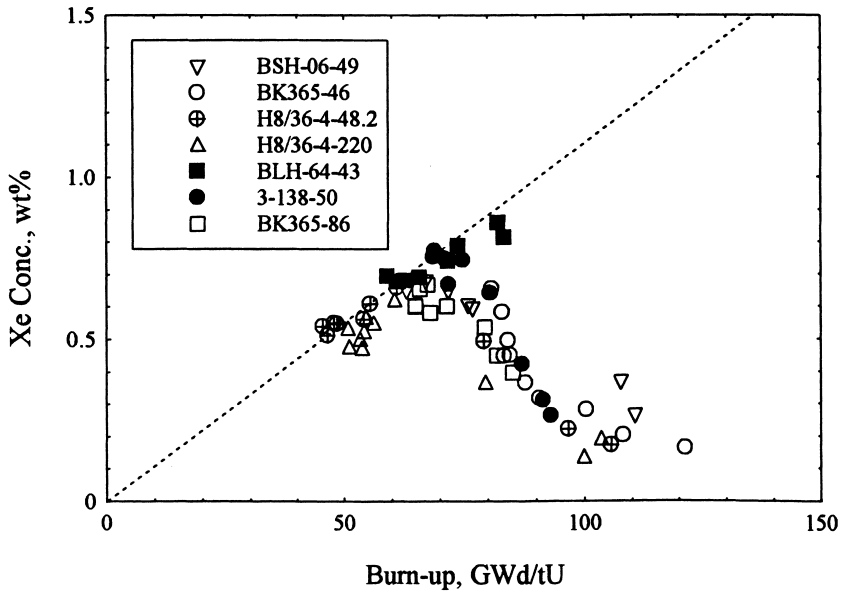

Fig. 9. Local concentration of xenon measured by EPMA in the outer region of the fuel between $r/r_o = 0.7$ and the pellet rim as function of the local burn-up. The xenon concentration falls beyond 60–75 GWd/tU due to the formation of the high burn-up structure. The dashed line represents the predicted relationship without release based on a hypothetical fission yield of 0.21. Note that the xenon concentration in section BLH-64-43 continues to climb with burn-up above 75 GWd/tU indicating the absence of the high burn-up structure.

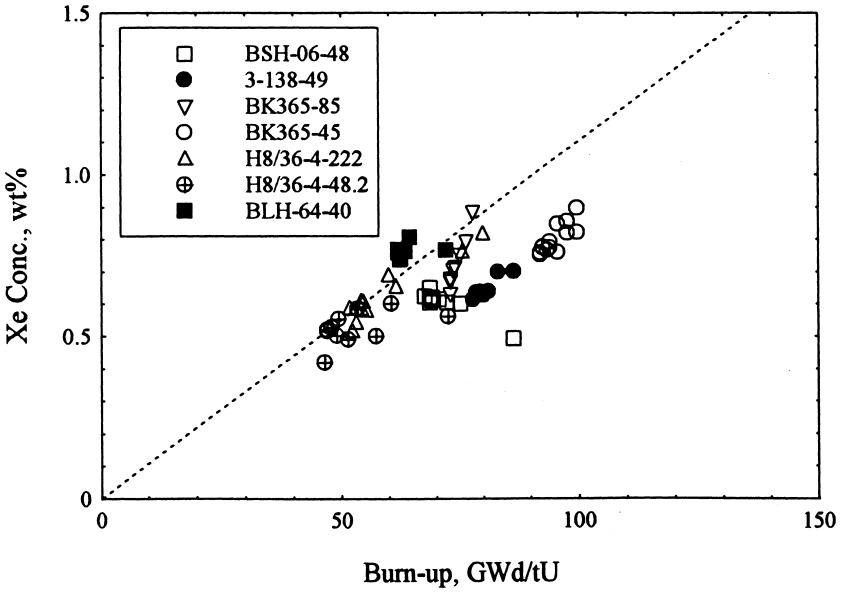

Fig. 10. Local concentration of xenon measured by XRF in the outer region of the fuel between $r/r_o = 0.7$ and the pellet rim as function of the local burn-up. The dashed line represents the predicted relationship without release based on a hypothetical fission yield of 0.21. In the rim region of sections 3-138-49 and BK365-45 at the locations where XRF indicated gas release the local burn-up was higher than 75 GWd/tU.

Fuel section BLH-64-43 represents the exception to this finding. As seen from Fig. 9 the xenon concentrations measured in the outer region of this section continue to increase with burn-up beyond 75 GWd/tU confirming that the high burn-up structure had not formed to the usual extent in this large grain fuel.

7.3. Fission gas release from the high burn-up structure to the rod free volume

As seen from Figs. 4, 5 and 7, the xenon concentrations measured by XRF in the rim region of the fuel sections BK365-85, 3-138-49, and BK365-45 all lie below the line representing the created amount. When the uncertainty on the XRF measurements is taken into account, however, only the disparities between the created amount of xenon and the retained amount measured by XRF in the sections 3-138-49 and BK365-45 are found to be statistically significant. It is, therefore, reasonable to assume that in these two sections fission gas had been released from the high burn-up structure to the rod free volume. For section BK365-45, this assumption is supported by the puncturing result for the rod which revealed that the plenium contained an appreciable amount of fission gas (see Table 8) although the fuel temperature had not exceeded the threshold for thermal fission gas release. From Fig. 10 it is seen that in the rim region of the fuel sections 3-138-49 and BK365-45 at the locations where XRF indicated fission gas release from the high burn-up structure the local burn-up was greater than 75 GWd/tU.

It is evident from Fig. 6 that fission gas release had also occurred from the high burn-up structure in fuel section BSH-06-48. In this case, however, the level of release may have been enhanced by the presence of islands of high ^{235}U enrichment in the fuel (see Section 3.1) which resulted in local areas with exorbitant high burn-up. The fuel microstructure in the outer region of the pellet is shown in Fig. 11. Holes resulting

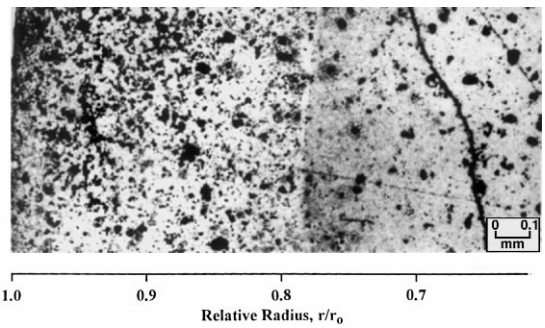

Fig. 11. Photomicrograph showing the microstructure of the fuel in the outer region of section BSH-06-49. Holes resulting from burn out of the islands of high ^{235}U enrichment are clearly visible. Extensive grain loss has occurred between the pellet rim and $r/r_o = 0.85$ during specimen preparation. Etchant: 10% H_2SO_4 in concentrated H_2O_2 solution.

from burn-out of the high enriched islands are clearly visible. In addition, extensive grain loss is evident in the vicinity of the pellet edge. Islands of high ^{235}U enrichment were also present in the large grain fuel in rod BLH-64, but since the high burn-up structure had not formed no gas was released in the outer region of the fuel.

7.4. Percentage of fission gas released

Details of the percentages of xenon released from the pellet cross-sections and from the outer region of the pellets are given in Table 8. The table contains both EPMA and XRF results for these quantities. The former represents the percentage of release from the UO_2 grains, whereas the latter is the percentage released to the rod free volume. Also included in the table are average release values for the rods obtained from puncturing. In principle, some similarity between the puncture results and the percentages of release measured by XRF is to be expected. The degree of agreement obtained, however, depends on the shape of the axial power profile and the axial position of the fuel section on which XRF was carried out [4]. Good agreement should be obtained when the power profile is flat.

From Table 8 it is evident that the percentage of gas released from the UO_2 grains in the outer region of the fuel was generally small compared with the percentage released from the pellet cross-section. Exceptions to this finding are provided by the two sections from rod BK365. As seen from the table, close to 90% of the gas released from the fuel grains in section BK365-86 came from the outer region of the pellet and in the case of BK365-46 about two-third of the released gas came from the outer region of the pellet. Normally, in the central region of the fuel, fission gas release from the UO_2 grains is the result of thermally activated diffusion, but this is apparently not so in the case of section BK365-46. In this section the release in the central region of the fuel appears to result from the formation of the high burn-up structure in this region.

In Table 8, the difference between the XRF and EPMA results for the pellet cross-section release is mainly due to gas retention on the grain boundaries at intermediate radial positions. In the outer region of the BWR fuel H8/36-4, XRF indicates complete retention of fission gas. This is consistent with the current understanding that most, if not all, of the fission gas released from the fuel when the high burn-up structure forms is retained in the new pore structure. It is also seen that in the outer region of section BLH-64-43, EPMA indicates that much less than 1% of the fission gas inventory had been released from the UO_2 grains, although at the pellet rim the local burn-up had greatly exceeded the usual threshold burn-up value for the onset of the high burn-up structure. Only in the case of section BSH-06-48 was it possible from the XRF measurements to obtain a reliable value for the percentage of fission gas released from the high burn-up structure to the rod free volume. As indicated in the table, 6.5% of the fission gas inventory in the fuel cross-section was released from the outer region of section BSH-06-48 which approximates to one-third of the gas released from the fuel section.

The puncturing results in Table 8 reveal that the percentage of fission gas released to the fuel rod free volume was marginally higher in rod BSH-06 than in rod BLH-64 (8.4% compared with 6.2%). It seems that the difference in the level of release reflects the escape of gas from the high burn-up structure in the rim region of the fuel in rod BSH-06 as the radial Xe concentration profiles indicate that the thermal releases experienced early in life (after ca. 40% of the burn-up had been accumulated) are very similar. Moreover, it is highly probable that a large part, if not all, of the gas released to the plenum in rod BK365, which amounted to 3.8% of the fission gas inventory, had escaped from the high burn-up structure. This is deduced from the fact that gas release from the UO_2 grains in section BK365-86 (80%

Table 8
Percentage of xenon released from the pellet cross-section and the pellet outer region as revealed by EPMA and XRF

Fuel section	Burn-up (GWd/tU)	Percentage release [a]				
		Pellet cross-section		Pellet outer region [b]		Rod average [c]
		EPMA	XRF	EPMA	XRF	
BK365-45/46	83.1	42.5		26.6		3.8
BSH-06-48/49	72.2	28.3	20.0	6.4	6.5	8.4
3-138-49/50	70.4	20.6		6.7		2.6
BK365-85/86	67.1	12.9		11.4		3.8
BLH-64-40/43	62.5	20.9	11.4	0.6	0.0	6.2
H8/36-4-220.5/222	54.9	24.7	19.7	4.0	0.0	17.3
H8/36-4-48/48.2	44.8	25.4	15.1	4.0	0.0	17.3

[a] Percentage of the fission gas inventory in the fuel cross-section.
[b] Between $r/r_o = 0.7$ and the pellet surface.
[c] Puncture results after Cunningham et al. [12].

peak power) was almost entirely restricted to the rim region and from the finding that all the gas release in section BK365-46 (peak power) can be attributed to the formation of the high burn-up structure throughout the fuel pellet cross-section (see Section 7.1).

8. Conclusions

The high burn-up structure in the fuel sections examined by EPMA and XRF in the HBEP penetrated much deeper than initially reported. In section BK365-46 with a burn-up of 83.1 GWd/tU it extended over the whole cross-section of the annular pellet, although it was less prominent at intermediate radial positions. The local burn-up threshold for the formation of the high burn-up structure in the BWR fuel with a grain size of 6.6 μm and BR-3 fuels with a grain size of 16 μm lay in the range 60–75 GWd/tU. This burn-up range is the same as that found for commercial PWR fuel. The high burn-up structure was not detected by EPMA, however, in the two fuel sections from rod BLH-64 which contained fuel with a grain size of 78 μm obtained by the addition of 0.46 wt% Nb_2O_5 although the local burn-up at the pellet rim had exceeded 80 GWd/tU. This finding constitutes important evidence that the transformation of the microstructure can be shifted to higher burn-up.

In rods 3-138, BSH-06 and BK365 fission gas had been released from the high burn-up structure to the rod free volume. In the rim region of the sections 3-138-49 and BK365-45, at the locations where XRF indicated gas release the local burn-up was higher than 75 GWd/tU. The percentage of release involved appears to be small. For example, in the case of rod BK365, slightly less than 4% of the fission gas inventory of the fuel cross-section was released to rod free volume, although the formation of the high burn-up structure was responsible for approximately 43% release from the fuel grains in section 46 (peak power) and about 11% release from the fuel grains in section 86 (80% peak power). In the case of section BSH-06-48, apparently all of the gas released from the UO_2 grains in the region where the high burn-up structure had formed, which amounted to 6.5% of the cross-section inventory, had escaped from the fuel. In this case, however, gas release may have been enhanced by a fabrication anomaly; namely, the presence of islands of high ^{235}U enrichment in the fuel.

References

[1] P. Knudsen, C. Bagger, H. Carlsen, B.S. Johansen, M. Mogensen, I. Misfeldt, Proceedings of the ANS Topical Mtg. on LWR Fuel Performance, Williamsburg, USA, 1988, p. 189.
[2] P. Knudsen, C. Bagger, M. Mogensen, H. Toftegaard, Proceedings of the Technical Committee on Fission Gas Release and Fuel Rod Chemistry Related to Extended Burnup, Pembroke, May 1992, IAEA-TECDOC-697, 1993, p. 193.
[3] M. Mogensen, J. Als-Nielsen, N.H. Andersen, Determination of fission products on irradiated fuel by X-ray fluorescence, Report Risø M-2599, 1986.
[4] M. Mogensen, C. Bagger, C.T. Walker, J. Nucl. Mater. 199 (1993) 85.
[5] M.E. Cunningham, M.D. Freshley, D.D. Lanning, J. Nucl. Mater. 200 (1993) 24.
[6] K. Lassmann, C.T. Walker, J. van de Laar, F. Lindström, J. Nucl. Mater. 226 (1995) 1.
[7] C.T. Walker, T. Kameyama, S. Kitajima, M. Kinoshita, J. Nucl. Mater. 188 (1992) 73.
[8] J. Rest, G.L. Hofman, J. Nucl. Mater. 210 (1994) 187.
[9] K. Nogita, K. Une, J. Nucl. Mater. 231 (1996) 32.
[10] J. Spino, C. Vennix, M. Coquerelle, J. Nucl. Mater. 231 (1996) 179.
[11] J.O. Barner, M.E. Cunningham, M.D. Freshley, D.D. Lanning, Nucl. Technol. 102 (1993) 210.
[12] M.E. Cunningham, M.D. Freshley, D.D. Lanning, J. Nucl. Mater. 188 (1992) 19.
[13] C. Bagger, M. Mogensen, C.T. Walker, J. Nucl. Mater. 211 (1994) 11.
[14] M.E. Cunningham and C.E. Beyer, GT2R2: An Updated Version of GAPCON-THERMAL-2, Pacific Northwest Laboratory Report PNL-5178 (NUREG/CR-307) (1984).
[15] C.T. Walker, J. Nucl. Mater. 80 (1979) 190.
[16] M. Mogensen, Int. J. Mass. Spect. Ion Phys. 48 (1983) 389.
[17] K. Une, K. Nogita, S. Kashibe, M. Imamura, J. Nucl. Mater. 188 (1992) 65.
[18] K. Nogita, K. Une, J. Nucl. Sci. Technol. 31 (1994) 929.
[19] K. Une, I. Tanabe, M. Oguma, J. Nucl. Mater. 150 (1987) 93.